Growth and characterization of $Cu_2ZnSn(S,Se)_4$ thin films for solar cells

P.M.P. Salomé, J. Malaquias, P.A. Fernandes, M.S. Ferreira, A.F. da Cunha, J.P. Leitão, J.C. González, F.M. Matinaga

ABSTRACT

Cu_2ZnSnS_4 (CZTS) and $Cu_2ZnSnSe_4$ (CZTSe) with their band gap energies around 1.45 eV and 1.0 eV, respectively, can be used as the absorber layer in thin film solar cells. By using a mixture of both compounds, $Cu_2ZnSn(S,Se)_4$ (CZTSSe), a band gap tuning may be possible. The latter material has already shown promising results such as solar cell efficiencies up to 10.1%. In this work, CZTSSe thin films were grown in order to study its structure and to establish the best growth precursors. SEM micrographs reveal an open columnar structure for most samples and EDS composition profiling of thecross sections show different selenium gradients. X-ray diffractograms show different shifts of thekesterite/stannite (1 1 2) peak, which indicate the presence of CZTSSe. From Raman scattering analysis, it was concluded that all samples had traces of CZTS and CZTSSe. The composition of the CZTSSe layer was estimated using X-ray diffraction and Raman scattering and both results were compared. It was concluded that Se diffused more easily in precursors with ternary Cu–Sn–S phases and metallic Zn than in precursors with ZnS and/or CZTS already formed. It was also showed that a combination of X-ray diffraction and Raman scattering can be used to estimate the ratio of S per Se in CZTSSe samples.

Keywords:
Cu2ZnSnSe4 (CZTSe), Cu2ZnSnS4 (CZTS), Cu2ZnSn(S,Se)4 (CZTSSe), Thin film solar cells, Kesterites, Chalcogenides

1. Introduction

The development of Cu_2ZnSnS_4 (CZTS) and $Cu_2ZnSnSe_4$ (CZTSe) solar cells have reached efficiencies up to 8.4% [1] and 3.2% [2], respectively. In 2011 Todorov et al., achieved an efficiency of 10.1% by preparing solar cells with an absorber layer of $Cu_2ZnSn(S,Se)_4$ (CZTSSe) [3]. These results heightened the interest in studying films with a mixture of S and Se as a possible replacement for $Cu(In,Ga)Se_2$ in thin film solar cells since the use of the expensive and scarce element In is avoided.

CZTSSe should have its band gap energy between the one of CZTSe and of CZTS and it should increase with the replacement of Se with, S similar to the case of the chalcopyrite semiconductors, $CuInSe_2$ and $CuInS_2$. This analysis is not straightforward since the exact values of the band gap energy for CZTSe and CZTS are still a debated subject in the literature. For CZTSe, Matsushita et al. [4] and Wibowo et al. [5], refer a value between 1.44 eV and 1.56 eV, but Zoppi et al. report values around 0.9 eV [2]. In 2010, Ahn et al. [6] and Salomé et al. [7] reported a band gap energy close to 1 eV. For CZTS, the reported values range from 1.45 eV to 1.66 eV [8–10], but a value closer to 1.5 eV is widely accepted.

Regarding the CZTSSe crystalline structure, it should crystallize in the same structure as CZTS and CZTSe, which is either stannite, *I*-42*m* group 121, or kesterite, *I*-4*m* group 82. The structures are similar, differing only in the ordering of Zn and Cu atoms. Since these atoms have very similar X-ray scattering factors, the identification of the crystalline structure is not possible using conventional X-ray diffraction (XRD) [11] and hereafter we will be considering only the kesterite structure. Concerning the CZTSSe lattice parameters, they should be between the ones of CZTSe and of CZTS. Thus, it is expected that in XRD patterns the peaks suffer angular displacements for different atomic ratios of [Se]/[S], for instance the (1 1 2) peak, should be between 27.16 and 28.44.

In this study, CZTSSe thin films were prepared and were structurally and morphologically characterized. Different types of precursors were used to allow one to decide which may be the best growth procedure for the formation of CZTSSe. A method to estimate the composition of the CZTSSe layer using both XRD and Raman scattering is studied and discussed.

2. Experimental details

2.1. Sample preparation

For the growth of CZTSSe, precursors containing sulphur were selenised. Different types of films were selenized namely,

Table 1
CZTSSe samples' growth details.

Sample number	Evaporated precursors	Sulphurization for the formation of CTS	Zn/ZnS Layer deposited	Sulphurization for the formation of CZTS	Selenization
1	Zn/Sn–S/Cu	No	–	No	Yes
2	SnS/CuS	Yes	Zn	Yes	Yes
3	SnS/CuS	Yes	ZnS	Yes	Yes
4	SnS/CuS	Yes	ZnS	No	Yes
5	SnS/CuS	Yes	Zn	No	Yes

metallic/sulphide precursors, ternary Cu_2SnS_3 (CTS)þZn/ZnS films and finally CZTS films. In Table 1, the growth details for each sample are presented. Depending on the samples, up to a maximum of five process steps were employed. First, precursors were evaporated and in a second step some of the samples were sulphurized to form CTS. The third step consisted on the deposition of a Zn or ZnS layer by RF magnetron sputtering. The fourth step was a sulphurization in order to form CZTS and finally the fifth step was the selenization to form the CZTSSe layer. Note that not all samples are subjected to the same steps.

In the first step, precursors were sequentially deposited on a Mo coated soda lime glass (SLG) in an evaporation system, with elemental sources of Sn, Cu, Zn and S, therefore allowing the deposition of different sulphides as well as metallic elements. The aimed thicknesses were 807 nm of $Cu_{2-x}S$ and 810 nm of SnS_2 which should provide a film with a [Cu]/[Sn] value close to 2.

In the second step, a tubular furnace was used [10]. The samples were heated up to a maximum temperature of 525 1C in a N_2 flow rate of 40 ml min^{-1}, at an operating pressure of 10 mbar. This pressure was used in order to minimize Sn losses by evaporation. The sulphur evaporation source was a quartz tube filled with elemental S pellets. The evaporation of sulphur was done at 130 1C. The purpose of this step, which was done prior to the incorporation of Zn, was the formation of a Cu–Sn–S phase, probably cubic Cu_2SnS_3 [12], in order to avoid Sn losses [13,14].

In the third step, either Zn or ZnS was deposited by RF magnetron sputtering. The deposition was performed in an Ar atmosphere at a working pressure of 2×10^{-3} mbar. The power densities for Zn and ZnS were 0.41 W cm^{-2} and 0.33 W cm^{-2}, respectively. In situ thickness monitoring was ensured by a quartz crystal monitor and it was aimed to deposit 220 nm of Zn or 570 nm of ZnS. These thicknesses were then confirmed by step profilometry. The fourth step was a sulphurization done in the same conditions as the second step. The final step to form the CZTSSe was a selenization done at a pressure of 1 mbar under an atmosphere of 95% N_2 and 5% H_2 and substrate temperatures of 525 1C [7].

The differences between the samples are precursor layers and on the processing steps prior to the selenization are shown in detailed in table 1. Sample 1 had metallic layers of Zn and Cu, S was only present during the evaporation of Sn with the following order: SLG/Mo/Zn/Sn–S/Cu. This sample was only selenized and the remaining steps were skipped. In the case of the other four samples, the second step to form CTS was performed. In sample 2, after the second step elemental Zn was deposited by RF sputtering and CZTS was formed before the selenization. In sample 3 instead of Zn, ZnS was deposited and CZTS was formed before the final selenization. In samples 4 and 5 after the second step ZnS and Zn were deposited, respectively. In both samples, the step to form CZTS was skipped. All samples were selenized under the same conditions.

These samples allowed us to investigate the structural properties of the different thin films and from their comparison to conclude which is the growth procedure most suitable for the growth of CZTSSe.

2.2. Sample characterization

The cross section of the resulting films was analysed by scanning electron microscopy (SEM) and energy dispersive spectrometry (EDS), the system was a SU-70 Hitachi with a Rontec EDS system and the acceleration voltage used was 25 kV. These measurements can both reveal important information about the morphology and chemical composition of the samples. Conventional EDS however is not capable of providing quantification for the content of S due to the fact that the X-ray emission lines of Mo and S are superimposed. The X-ray emission lines are 2.29 keV for the L_a line of Mo and 2.30 keV for the K_a line of S. One could lower the acceleration voltage so that the Mo layer is not included in the interaction volume, but, in that case, the quantification of Zn and Cu is not ideal since the Cu and Zn L_a lines nearly overlap around 0.9 keV. Since we are dealing with structured layers, the conditions to perform EDS are also not ideal.

The crystalline structure was studied by X-Ray Diffraction (XRD) with X'Pert MPD Philips diffractometer using the Cu K_a line (1.5419 Å). The XRD allows the estimation of the incorporation of Se by looking at the shift of the kesterite (1 1 2) peak. It is known that for CZTSe this peak is centred at 27.161 and for CZTS is centred at 28.441 thus, for CZTSSe, it is expected that the (1 1 2) peak lies between the values above. The expected peak positions mentioned in this paper are taken from the International Centre for Diffraction Data (ICDD).

The films were also analysed by Raman scattering at room temperature using a Jobin-Yvon T64000 micro-Raman spectrometer equipped with a liquid nitrogen cooled silicon CCD and a BX51 Olympus optical microscope. It was used a 100X objective with a 0.95 numerical aperture to excite and collect the Raman signal in the backscattering configuration. The samples were excited with the 532 nm line of a Verdi™ DPSS laser at 2 mW of excitation power on the sample.

3. Results and discussion

The results of the EDS mapping analysis, with the Se counts in the cross sections, are shown in Fig. 1. The cross section SEM micrographs are also shown. This analysis reveals that for all samples, Se was mainly concentrated in a thin layer close to the surface. These results indicate that the Se diffusion was low. For a more thorough analysis other techniques such as SIMS would be needed. The morphology of the resulting CZTSSe films is depicted in Fig. 2. Sample 1 is the most compact one, showing large grains at the top and smaller ones close to the back. The other four samples share a similar columnar structure. In the case of sample 2 just the columnar structure is observed whereas for sample 3 voids are also present. The micrograph for the latter sample, which had ZnS deposited and CZTS was formed, shows a layer at the top of the sample. Sample 4 has the generic structure that all the other samples show but, at the top, it appears to have a different layer. For this sample ZnS was deposited, and CZTS was

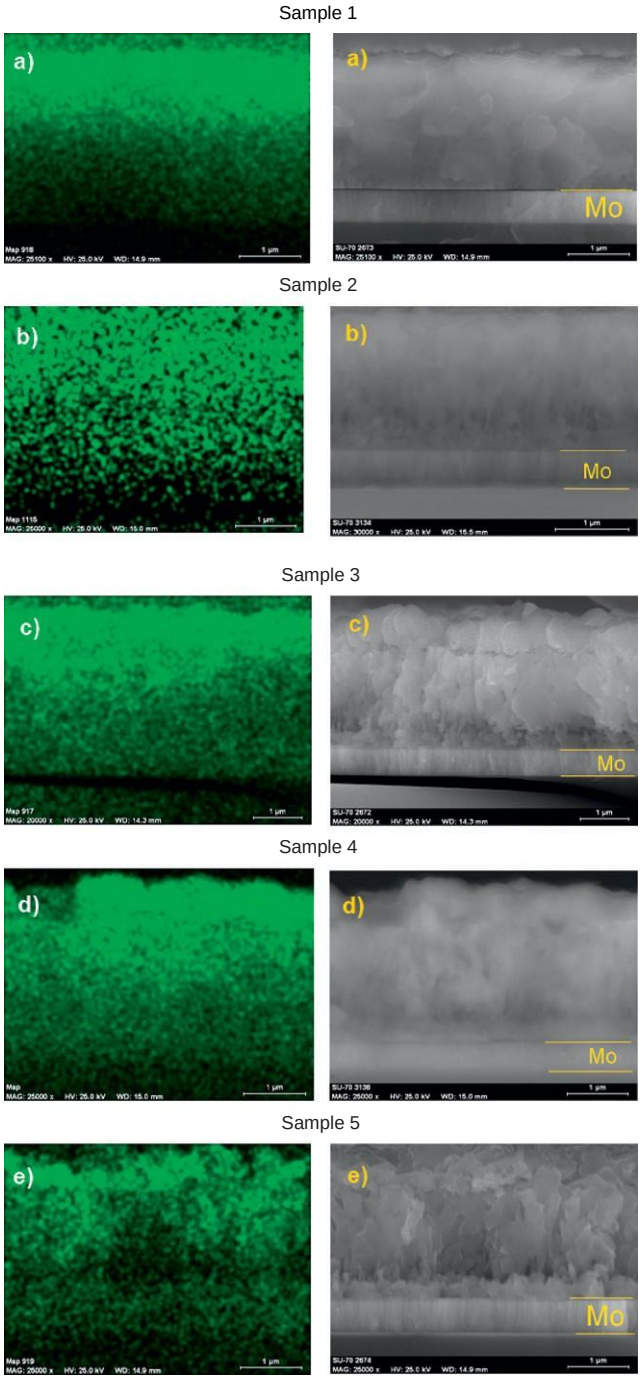

Fig. 1. EDS mapping showing the distribution of Se in the cross section of the CZTSSe samples and the corresponding SEM micrographs of the secondary electrons: (a) sample 1, (b) sample 2, (c) sample 3, (d) sample 4 and (e) sample 5. In the cross section micrograph, the Mo layer is identified.

not formed. Sample 5 has larger grains than samples 2–4, but the voids are bigger as well.

In order to evaluate the [*S*]/([*S*] þ [Se]) ratio in the grown thin films and to try to evaluate which phases are present, XRD measurements were performed and the full diffractograms are presented in Fig. 3. All samples show clearly the presence of Mo as well as of a CZTS phase. For the CZTSe phase, only in samples 1 and 5 some of the peaks related to this phase are observed. The identification of CZTS and CZTSe in our samples cannot be rejected by the possible presence of spurious phases like $Cu_2Sn(S,Se)_3$ and Zn(S,Se). The identification can be done since some of the kesterite peaks that are not superimposed with the peaks of those spurious phases can be seen: (1 0 1) reflection for CZTSe (17.42l) or for CZTS (18.24l); (1 1 0) reflection for CZTSe (22.08l) or for CZTS (23.12l); (2 1 1) reflection for CZTSe (36.15l) or for CZTS (37.90l). Considering the positions of the main peaks for the CZTSe and CZTS phases, namely, for the reflections (1 1 2) at "'27–28.5l, (2 0 4) at "'45–47.4l and (3 1 2)/(1 1 6) at "'54–56.3l, our samples show the presence of several peaks between the ones for the CZTSe and CZTS phases. Their relative intensities change depending on the film under analysis, which should be related to the growth procedure for each sample. These results allow us to assume the presence of a kesterite $Cu_2ZnSn(S,Se)_4$ layer in our samples. Since a Se diffusion profile has been observed using the EDS mapping, see Fig. 1, it is very likely that this complex broad peak structure between all the CZTSe and CZTS peaks is from a Se grading from top to bottom in the different films. This diffusion profile along with the strong CZTS XRD peaks shows that the pure layer of CZTS is located at the bottom part of the samples. The previous peak positions and attributions to the crystallographic direction were correlated using the International Centre for Diffraction Data [15].

Due to the complex task of analysing all the peaks, we will focus on the (1 1 2) peaks since it is the range of angles where the reflection peaks have higher counts and so the analysis is simpler. A zoom of these peaks is shown in Fig. 4. The positions of the (1 1 2) peak for CZTSe at 27.16l and CZTS at 28.44l are shown as vertical lines for reference. All the samples present a strong peak between the CZTSe and CZTS peaks, therefore it will be assumed that this peak is due to a reflection from the (1 1 2) planes of the CZTSSe phase. This peak will be referred to as an intermediate peak since it is between the (1 1 2) peaks for CZTSe and for CZTS. Notice that in the ICDD XRD database, there are no entries for mixed S and Se materials as the ones we are dealing in this work. Assuming that the shift of the CZTSSe (1 1 2) peak follows a linear trend between the ones of CZTSe and CZTS, this peak position, *x*, could be used to estimate the [*S*]/([*S*]þ[Se]) content of the CZTSSe layer. That can be done using a linear interpolation of the position of the (1 1 2) peak in the kesterite structure, which is given by the following equation:

$$[S]/([S]+[Se]) = (x - 27.16)/A; \quad (1)$$

where *A* is a linear factor and takes the value 1.28, which results from the difference between the CZTS and CZTSe (1 1 2) peak positions, 28.44 and 27.16, respectively.

Sample 1 shows the well resolved CZTSe (1 1 2) peak, indicating the existence of a layer of CZTSe in its structure. This sample is the only one with the intermediate peak closer to the CZTSe than to the CZTS. The intermediate peak is also stronger than the CZTS or the CZTSe peaks. It is located at 27.51l which points to a [*S*]/([Se]þ[*S*]) ratio around 27%. From these observations one can say that this sample is comprised by at least three different layers, CZTS, CZTSSe and CZTSe. Although this sample had the largest grains, one cannot say that this is due only to the influence of Se since the precursor of this sample was different from remaining ones.

Sample 2 shows a strong CZTSe peak at 27.95l and along with sample 1, this peak is stronger than the CZTS peak. Using Eq. (1), this position points to a CZTSSe compound with 60% of S and 40% of Se. Additionally, a shoulder centred at "'27.65l suggests the presence of a CZTSSe phase with a [*S*]/([Se]þ[*S*]) value around 40%.

The lower intensity ratio between the CZTSSe and CZTS (1 1 2) peaks for sample 3 may indicate that there was a smaller incorporation of Se. However, there still is an intermediate peak located at 27.68l which may indicate a CZTSSe phase with a ratio [*S*]/([Se] þ [*S*]) of 40%. A broadening of the CZTS (1 1 2) peak for higher angles is also observed. The origin of this broadening could be related to the presence of a small amount of ZnS for which the

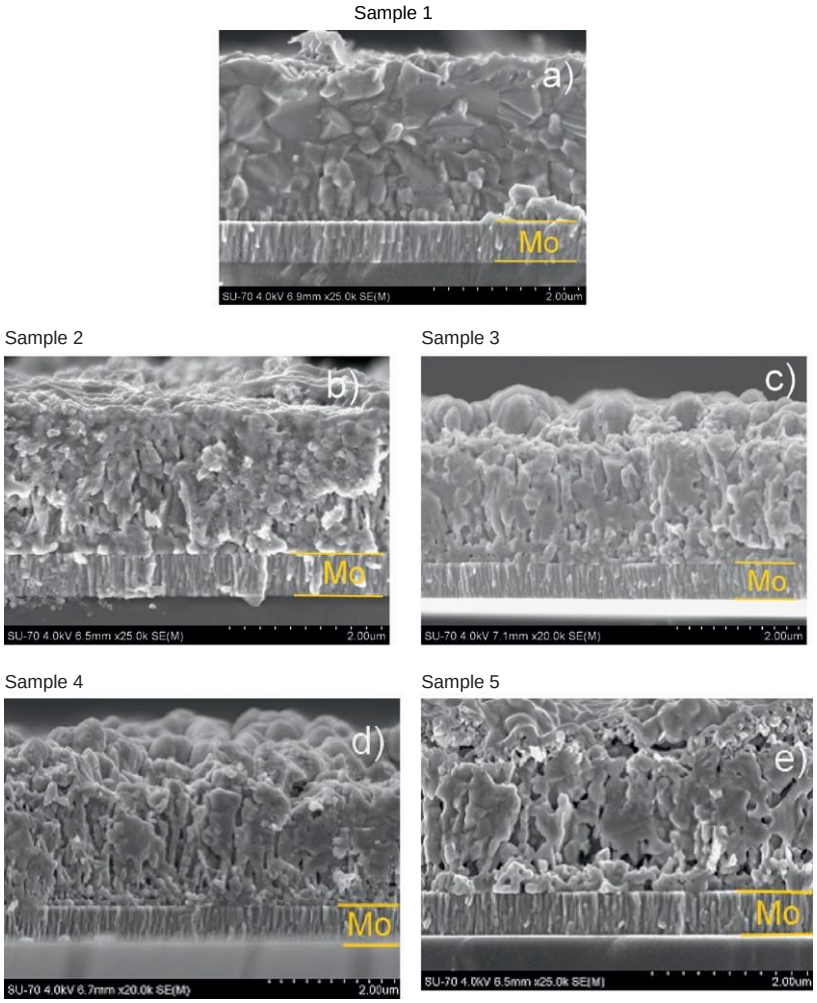

Fig. 2. SEM micrograph of the cross section of the various CZTSSe samples, (a) sample 1, (b) sample 2, (c) sample 3, (d) sample 4 and (e) sample 5. The Mo layer is identified.

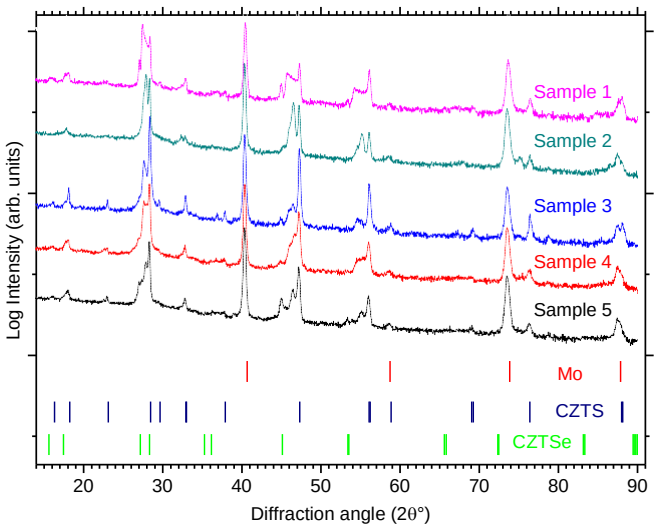

Fig. 3. Full XRD diffractograms of samples 1 to 5. The positions of the Mo, CZTS and CZTSe peaks are identified at the bottom of the figure.

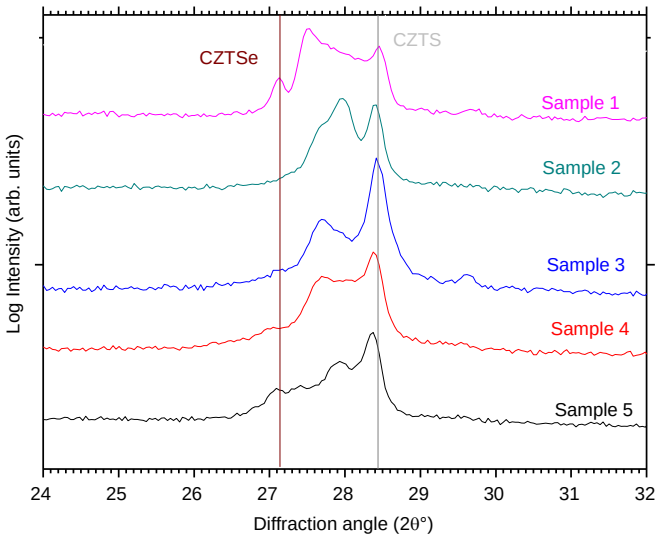

Fig. 4. XRD diffractograms centred at the (1 1 2) reflection kesterite peak for samples 1 to 5.

main diffraction peak, (1 1 1), is located at 28.57. However, no definitive conclusions can be drawn regarding the presence of ZnS due to the small angle difference.

Sample 4 showed in the SEM micrograph a different morphology at the top, which could be ZnS, however, no significant shoulder was visible near the CZTS (1 1 2) peak. The EDS mapping

shows a high concentration of Se at the top. Thus, the difference in the morphology could come from the Se incorporation or from the formation of Zn(*S*,Se) compounds which may give rise to peaks between the ones of CZTSe and CZTS. In this sample a peak can be found at 27.71 which could be from a CZTSSe phase with a ratio [*S*]/([Se]þ[*S*]) of 40%.

As mentioned before, sample 5 has a peak at 27.161 which indicates that CZTSe is present. From all the studied samples, this is the one that appears to have a smoother gradient of Se since the intensity of the peaks lowers continuously from the CZTS to the CZTSe (1 1 2) peak. There are two visible intermediate peaks, located at 27.391 and 27.921 which correspond to a ratio [*S*]/([Se]þ[*S*]) of 17% and 60%, respectively. However, the EDS results for this sample do not confirm the presence of a Se gradient.

Raman scattering measurements on the cross sections would allow a more detailed discussion regarding the origin of the XRD peaks. However, such measurements are hard to perform due to the large size of the laser spot, which is approximately 1 mm wide, and due to the difficulty in correctly focusing it. Instead, surface Raman scattering analysis was performed since additional information on possible secondary phases can be obtained. According to the literature, the main peaks of the discussed phases are found at: 194–197 cm^{-1} for CTZSe [16,17], 250 cm^{-1} for ZnSe [18], 260 cm^{-1} for $Cu_{2-x}Se$ [19], 334–338 cm^{-1} for CZTS [12], 350 cm^{-1} for ZnS [20] and 475 cm^{-1} for $Cu_{2-x}S$ [12]. In Fig. 5, the Raman scattering spectra is presented and the literature values for the peak positions of CZTSe, $Cu_{2-x}Se$ and CZTS are represented as vertical lines. All samples show a peak at 331 cm^{-1} which is attributed to the CZTS A1 mode. This peak appears shifted to lower energies with respect to the reported values, 338 cm^{-1}. This is not caused by a calibration problem since most of the samples show a $Cu_{2-x}Se$ peak at 262 cm^{-1}, which is in accordance with the literature. The exact same shift to lower energies of the CZTS peak for all the samples is not fully understood, but it may be due to a gradient in strain [21], due to a gradient of crystal quality in the layers [22] or even heating of the samples [23]. This peak is strongly related to CZTS since its presence was confirmed by XRD measurements, as discussed previously. Furthermore no other secondary phases are known to have a Raman scattering peak at the referred position, 331 cm^{-1}. According to Grossberg et al. [24], the A1 vibration mode of the CZTS shifts to lower energies with the substitution of S by Se, but for all samples

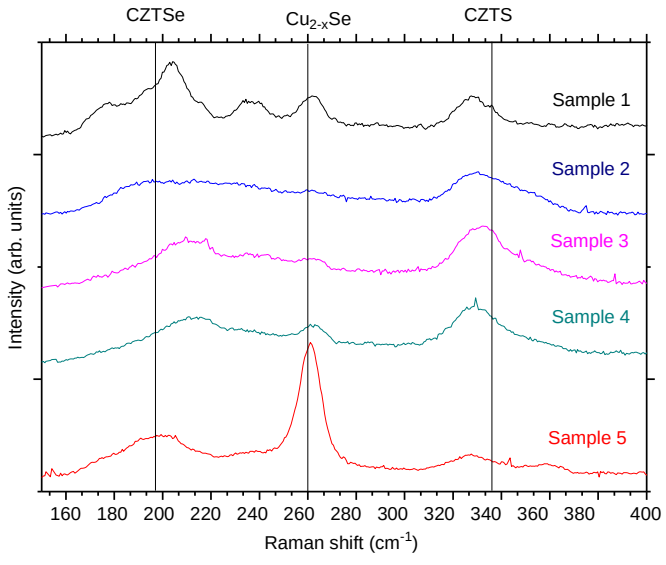

Fig. 5. Raman scattering analysis of the CZTSSe thin films. The vertical lines are guides to the eye corresponding to the main Raman scattering peaks of the referred structures.

the peak is located at the same value, thus the shift is not due to different Se contents but to other reason. However, in this study we are dealing with graded films whereas Grossberg et al. [24] analysed bulk homogenous samples. For all samples one or more peaks are present in the spectra in the range 200–250 cm^{-1}. According to the results of Grossberg et al. [24] this vibration mode, an A1 mode, also shifts linearly with different replacement values of Se per S. Thus, it can be assumed that the shifting of these peaks is due to a replacement of Se atoms by S atoms. Given the values of the CZTSe A1 vibration mode published by Grossberg et al. [24], where it was presented a linear shift of this peak between 196 cm^{-1} and 226 cm^{-1} for samples with a ratio of [*S*]/([Se]þ[*S*]) from 0% to 75%, it is possible to correlate the composition of the analysed sample with its Raman peak position, *Z*, similar to what was done with XRD results, in this work, by using a linear interpolation:

$$[S]/([Se]+[S]) = (Z-196)/40; \quad (2)$$

where 196 is the peak position for a ratio of 0% and 40 is the linear constant that fits to Grossberg et al. results.

Therefore, and considering the XRD results, the peaks found between 196 cm^{-1} and 226 cm^{-1} can be associated with a CZTSSe phase.

Sample 1 shows the strongest CZTSSe peak, located around 204 cm^{-1} and along with sample 5 shows a CZTSSe peak stronger than the CZTS peak. This, however, does not mean that the sample has a higher content of CZTSSe compared to CZTS since the Raman scattering efficiency of the different materials may not be the same.

Samples 2 and 3, present a pronounced shoulder after 330 cm^{-1}, close to the CZTS main peak, at higher energies. As the main peak of ZnS is around 350 cm^{-1}, these shoulders may indicate that these samples have traces of ZnS, but since the peaks are quite broad, it is difficult to resolve Lorentz curves to try to figure out hidden peaks [25]. In XRD measurements, sample 3 was the one where the CZTS (1 1 2) peak, located at 28.441, presented a higher shift in the direction of the (1 1 1) ZnS peak at 28.571. So, XRD and Raman data suggest the presence of ZnS in sample 3.

Most of the samples show the 262 cm^{-1} peak of $Cu_{2-x}Se$ and sample 5 is the one where this peak has the highest relative intensity. This identification also explains the XRD peak found at 27.921 since CuSe has a XRD maximum located at 28.021. No traces of $Cu_{2-x}S$ were found. The presence of $Cu_{2-x}Se$ and Se at the surface, as revealed by the EDS measurements, suggest that the film is Cu rich at the surface. The Raman peaks shown are broad which may reveal a poor crystalline quality. Regarding the presence of Zn(S,Se) in samples 3 and 4, both had a layer of ZnS deposited and showed a layer with different morphology on top of the processed film. However this was not confirmed since at the Raman ZnSe peak position, 250 cm^{-1}, nothing is found and the presence of ZnS was already discussed. A better look at the different layers would be possible by either using different excitation wavelengths [25], or by using a UV laser along with sputtering to perform an in-depth Raman [26].

With the information from the XRD and the Raman a comparison of the compositions of the CZTSSe phases obtained by the two methods was done and is presented in Table 2. For samples 1,3,4 and 5 the composition of the CZTSSe phases found by XRD and Raman are in good agreement. For sample 2, there are two intermediate XRD peaks and thereby two compositions can be estimated, 40% and 60% for the ratio [S]/([Se]þ[S]). However, the Raman scattering shows a structure of peaks between 197 cm^{-1} and 230 cm^{-1} which would correspond to a value of [*S*]/([Se]þ[*S*]) between 0 and 80. Considering both results, one can say that probably there are several CZTSSe phases, which is similar to say that there is a strong Se grading. The errors of the estimation of [*S*]/([Se]þ[*S*]) depend mostly on the broadening of the peaks for both techniques. Since the source of this broadening

Table 2
Raman and XRD peak positions for the CZTSSe phase vibration mode and (1 1 2) reflection, respectively. The comparison of the ratio [*S*]/([Se]þ[*S*]) for the CZTSSe phase estimated using Raman scattering (Eq. (2)) and XRD (Eq. (1)) are also shown.

Sample	Raman scattering CZTSe A1 vibration mode (cm^{-1}) (*z*)	XRD intermediate peak positions (1) (*x*)	Estimated XRD [*S*]/([Se]þ[*S*]) (%)	Estimated Raman [*S*]/([Se]þ[*S*]) (%)
1	204	27.51	27	20
2	197–230	27.65	40	0–80
		27.95	62	
3	210–217	27.68	40	35–52
4	212–216	27.70	42	40–50
5	200–204	27.39	17	15–20

is coming from a graded structure, and our estimation is based on a single layer, they also depend mainly on the Se grading for each sample and less on the measuring technique itself. Therefore, a quantification of an uncertainty is hard.

From these structural and morphological analyses, there were two samples that presented more distinctive results: samples 1 and 5. The sample with the best morphology was sample 1 and it also revealed a strong intermediate peak closer to the CZTSe peak, both in XRD and in the Raman scattering analysis. It is possible that this sample had the highest Se content, due to the presence of the XRD CZTSe peak and to the fact that the XRD CZTSSe peak is located closer to the CZTSe position. The diffractogram of sample 5 shows a continuum of peaks between the CZTSe and CZTS (1 1 2) maxima, which suggests that it has the smoothest Se grading among all samples. In the Raman scattering analysis, the sample exhibited a strong $Cu_{2-x}Se$ peak, which explains one of the intermediate peaks of the XRD, but it also presented an intense CZTSSe peak when compared to the other samples. The fact that CZTS was not formed prior to the selenization and Zn was in its metallic form, was probably a determining factor in allowing the diffusion of Se into the film. Regarding the two samples where CZTS was formed before the selenization, samples 2 and 3, they both presented strong XRD CZTS peaks and it is even likely that sample 3 had a ZnS layer. From a previous work [27], we already knew that preparing the precursors with a ZnS layer without the presence of H_2, leads to CZTS films with some ZnS on top. In the present work, H_2 was used during the selenization step instead of the sulphurization step which may have influenced the results; moreover, the evidences of the ZnS layer are not as strong as in the previously mentioned work. Sample 4, the one where CZTS was not formed and ZnS was deposited, showed a Se ratio close to 50%, small traces of $Cu_{2-x}Se$ and no traces of ZnS were found.

4. Conclusions

In this work, we have studied the incorporation of Se into different samples to evaluate the best route for the formation of CZTSSe thin films. It was evidenced that in samples where ZnS or CZTS was formed prior to the selenization, the incorporation of Se was smaller than in precursors with metallic layers or in precursors where there was only CTS and elemental Zn. It was proved that in all samples, a Se graded structure was produced with different ratios of incorporation of Se. If one intends to have a large amount of Se introduced in these films, without the appearance of secondary phases, then the use of precursors with Mo/Zn/SnS/Cu or Mo/SnS/CuS/ZnS without the formation of CZTS are the most suitable choices.

It was also shown that the XRD and Raman scattering peak positions shift with the quantity of Se incorporated and a comparison of the estimated composition determined by XRD and Raman scattering of the CZTSSe layer was done. This is in accordance with other published work [28]. Using the equations developed in this paper, the two techniques can be used to estimate the quantity of Se and S, something that is not possible to do using conventional EDS due to the overlapping of the Mo L_a and S K_a emissions.

Acknowledgements

The authors would like to thank the bilateral collaboration project FCT/DAAD with the HZB. Alfons Weber, Christiane Stephan, and Bjo¨rn-Arvid Schubert are acknowledged for the help with the preparation of the precursors.

P. A. Fernandes acknowledges the financial support of FCT, through a Ph.D. grant number SFRH/BD/49220/2008. FCT is also acknowledged for support given by the project PEst-C/CTM/LA0025/2011 and for supporting the national network of microscopy through FCT: REDE/1509/RME/2005. J. C. Gonza´lez, F. M. Matinaga, G. M. Ribeiro and E. R. Viana thank the support of CNPq, CAPES and FAPEMIG. This work was also funded by FCT through a grant, from its program COMPETE/FEDER, number PTDC/CTM-MET/113486/2009.

References

[1] B. Shin, O. Gunawan, Y. Zhu, N.A. Bojarczuk, S.J. Chey, S. Guha, Thin film solar cell with 8.4% power conversion efficiency using an earth-abundant Cu_2ZnSnS_4 absorber, Progress in Photovoltaics: Research and Applications . (2011). 10.1002/pip.1174.

[2] G. Zoppi, I. Forbes, R.W. Miles, P.J. Dale, J.J. Scragg, L.M. Peter, $Cu_2ZnSnSe_4$ thin film solar cells produced by selenisation of magnetron sputtered precursors, Progress in Photovoltaics: Research and Applications 17 (2009) 315–319.

[3] D. Aaron R. Barkhouse, Oki Gunawan, Tayfun Gokmen, Teodor K. Todorov and David B. Mitzi, Device characteristics of a 10.1% hydrazine-processed $Cu_2ZnSn(Se,S)_4$ solar cell, Progress in Photovoltaics: Research and Applications . (2011)10.1002/pip.

[4] H. Matsushita, T. Ichikawa, A. Katsui, Structural, thermodynamical and optical properties of Cu_2-II–IV–VI_4 quaternary compounds, Journal Of Materials Science 40 (2005) 2003–2005.

[5] Rachmat Adhi Wibowo, Woo Seok Kim, Eun Soo Lee, Badrul Munir, Kyoo Ho Kim, Single step preparation of quaternary $Cu_2ZnSnSe_4$ thin films by RF magnetron sputtering from binary chalcogenide targets, Journal of Physics and Chemistry of Solids 68 (2007) 1908–1913.

[6] SeJin Ahn, Sunghun Jung, Jihye Gwak, Ara Cho, Keeshik Shin, Kyunghoon Yoon, Doyoung Park, Hyonsik Cheong, Jae Ho Yun, Determination of band gap energy (Eg) of $Cu_2ZnSnSe_4$ thin films: on the discrepancies of reported band gap values, Applied Physics Letters 97 (2010) 021905.

[7] P.M.P. Salome´, P.A. Fernandes, A.F. da Cunha, J.P. Leita~o, J. Malaquias, A. Weber, J.C. Gonza´lez, M.I.N. da Silva, Growth pressure dependence of $Cu_2ZnSnSe_4$ properties, Solar Energy Materials & Solar Cells 94 (2010) 2176–2218.

[8] Sang-Yul Jae-Seung Seol, Jae-Choon Lee, Hyo-Duk Lee, Kyoo-Ho Namb, Kima, Electrical and optical properties of Cu_2ZnSnS_4 thin films prepared by rf magnetron sputtering process, Solar Energy Materials & Solar Cells 75 (2003) 155–162.

[9] Jonathan J. Scragg, Philip J. Dale, Laurence M. Peter, Guillaume Zoppi, Ian Forbes, New routes to sustainable photovoltaics: evaluation of Cu_2ZnSnS_4 as an alternative absorber material, Physica Status Solidi B Basic Solid State Physics 245 (9) (2008) 1772–1778. doi:10.1002/pssb.200879539.

[10] P.A. Fernandes, P.M.P. Salome´, A.F. da Cunha, Precursor's order effect on the properties of sulfurized Cu_2ZnSnS_4 thin films, Semiconductor Science and Technology 24 (2009) 105013. 7pp.
[11] S. Schorr, Structural aspects of adamantine like multinary chalcogenides, Thin Solid Films 515 (2007) 5985–5991.
[12] P.A. Fernandes, P.M.P. Salome´, A.F. da Cunha, Growth and Raman scattering characterization of Cu_2ZnSnS_4, Thin Solid Films 517 (7) (2009) 2519–2523.
[13] T.M. Friedlmeier, H. Dittrich, H.W. Schock, Growth and characterization of Cu_2ZnSnS_4 and $Cu_2ZnSnSe_4$ thin films for photovoltaic applications, The 11th Conference on Ternary and Multinary Compounds, ICTMC-11, Salford, 8–12 September, 1997, p.345.
[14] A. Weber, R. Mainz, H.W. Schock, On the Sn loss from thin films of the material system Cu–Zn–Sn–S in high vacuum, Journal of Applied Physics 107 (2010) 013516.
[15] International Centre for Diffraction Data; Cu_2ZnSnS_4 04-005-0388, $Cu_2ZnSnSe_4$ 04-010-6295.
[16] M. Altosaar, J. Raudoja, K. Timmo, M. Danilson, M. Grossberg, J. Krustok, E. Mellikov, $Cu_2Zn_{1-x}Cd_xSn(Se_{1-y}Sy)_4$ solid solutions as absorber materials for solar cells, Physica Status Solidi A Applications and Material Science 205 (1) (2008) 167–170.
[17] P.M.P. Salome´, P.A. Fernandes, A.F. da Cunha, Morphological and structural characterization of $Cu_2ZnSnSe_4$ thin films grown by selenization of elemental precursor layers, Thin Solid Films 517 (7) (2009) 2531–2534.
[18] G. Lermann, T. Bischof, A. Materny, W. Kiefer, T. K¨immell, G. Bacher, A. Forchel, G. Landwehr, Resonant micro-Raman investigations of the ZnSe–LO splitting in II–VI semiconductor quantum wires, Journal of Applied Physics 81 (3) (1997) 1446–1450.
[19] C. Xue, D. Papadimitriou, Y.S. Raptis, W. Richter, N. Esser, S. Siebentritt, M. Ch., Lux-steiner, micro-Raman study of orientation effects of CuSe-crystallites on Cu-rich $CuGaSe_2$ thin films, Journal of Applied Physics 96 (4) (2004) 1936–1966.
[20] J. Serrano, A. Cantarero, M. Cardona, N. Garro, R. Lauck, R.E. Tallman, T.M. Ritter, B.A. Weinstein, Raman scattering in þ-ZnS, Physical Review B 69 (2004) 014301.
[21] F.H. Pollak, M. Cardona, Effect of static uniaxial stress on the raman spectrum of silicon, Solid State Communications 8 (1970) 133–138.
[22] Gwe´nae¨l Gouadec, Philippe Colomban, Raman spectroscopy of nanomaterials: how spectra relate to disorder, particle size and mechanical properties, Progress in Crystal Growth and Characterization of Materials 53 (2007) 1–56.
[23] Guy Lucazeau, Effect of pressure and temperature on Raman spectra of solids: anharmonicity, Journal of Raman Specroscopy 34 (2003) 478–496.
[24] M. Grossberg, J. Krustok, J. Raudoja, K. Timmo, M. Altosaar, T. Raadik, Photoluminescence and Raman study of $Cu_2ZnSn(Se_xS_{1-x})_4$ monograins for photovoltaic applications, Thin Solid Films (2010). doi:10.1016/j.tsf.2010.12.099.
[25] P.A. Fernandes, P.M.P. Salome´ and A.F. da Cunha, Study of polycrystalline Cu_2ZnSnS_4 films by Raman scattering, Journal of Alloys and Compounds, doi:10.1016/j.jallcom.2011.04.097.
[26] X. Fontane´, L. Calvo-Barrio, V. Izquierdo-Roca, E. Saucedo, A. Pe´rez-Rodriguez, J.R. Morante, D.M. Berg, P.J. Dale, S. Siebentritt, In-depth resolved Raman scattering analysis for the identification of secondary phases: characterization of Cu_2ZnSnS_4 layers for solar cell applications, Applied Physics Letters 98 (2011) 181905.
[27] P.M.P. Salome´, J. Malaquias, P.A. Fernandes, M.S. Ferreira, J.P. Leita˜o, A.F. da Cunha, J.C. Gonza´lez, F.N. Matinaga, G.M. Ribeiro, E.R. Viana, The influence of hydrogen in the incorporation of Zn during the growth of Cu_2ZnSnS_4 thin films, Solar Energy Materials and Solar Cells (2011). doi:10.1016/j.solmat.2011.08.008.
[28] J. He, L. Sun, S. Chen, Y. Chen, P. Yang, J. Chu, Composition dependence of structure and optical properties of $Cu_2ZnSn(S,Se)_4$ solid solutions: an experimental study, Journal of Alloys and Compounds (2010). doi:10.1016/j.jallcom.2011.08.099.